Pattern Formation on Aluminum Electrodes

M. U. Kleinke, O. Teschke,* and M. A. Tenan

Instituto de Fisica-UNICAMP, 13081 Campinas SP, Brazil

ABSTRACT

The mechanisms of the cells forming the almost periodic structure on anodized aluminum electrodes in contact with various acid solutions was investigated. Their size was correlated to the product of the electrode wettability variation induced by switching the applied potential from a hydrogen evolution potential to an anodizing potential and the current density during the anodizing process. The mechanism of cell formation is related to solute concentration inhomogeneities at the film-solution interface generating local variations in the film-solution interfacial tension. Interfacial tension gradients induce spatial and temporal variations in the electrolyte velocity. Particles dragged by electrolyte motion will also have different velocities, so that interparticle contacts will occur. The internal motion of the fluid film accelerates the aggregation of particles into preferential geometries which were observed on the electrode surface by SEM. The size of cells forming the structure, for various acids and for various concentrations of sulfuric acid, were determined experimentally and a successful matching of these results with the model recently developed was obtained.

The anodic oxidation of aluminum is a technique which has been known for many years and which has found widespread industrial application (1, 2). Coatings can be formed in various electrolytes under a wide variety of forming conditions, and, as a result, exhibit characteristics and behavior which are many and varied. The produced covering layers are of two distinct types: porous or barrier type. The mechanism of pore formation, the actual part the electrolyte anions play, and the reason for the behavior of aluminum are not well understood. Many workers have studied the problem (3-11), suggesting that pore nucleation is due mainly to the influence of aluminum grain boundaries, surface inhomogeneities, or local heating. These theories have been reviewed extensively (1-12). Wernick (13) and Baumann (14) considered the role of the interface in the formation mechanism. Murphy and Michelson (15) have suggested that the oxide layer consists of colloidal particles which are free to rearrange under the influence of external forces. Heber (16) more recently postulated pockets in the colloidal layer as nuclei for the pore formation.

The film forming on the aluminum anode is subjected to many forces. Surface roughness, metallurgical inhomogeneities, and nonuniform electrolyte convection will certainly create a locally variable electrode current. There is, however, no reason why such irregular disturbances should lead to the regularity of pores without the help of some other mechanism. In this paper we consider surface phenomena at the electrode-electrolyte interface as the generator of pores.

Current density *vs.* time transient curves for the formation of a barrier-type and a porous-type anodic film on aluminum are shown in Fig. 1. The curves diverge at point A which is related to pore initiation phenomenon induced by fluid motion (1). A similar turbulent convection may be observed by optical microscopy for iron electrodes which present similarly shaped curves around the 100 mV *vs.* SCE region (17).

Pore Formation Theory

The model has been previously described (18) and will only be summarized here. Diffusion and convection-controlled oxide formation processes that take place at a bare metal surface exposed to an acid solution are considered. As the metal surface anodizes, the metal ion concentration in the electrolyte increases and eventually reaches such a critical supersaturation value that a precipitate film (16, 19) is formed on the anodizing surface. It is also considered that the reaction products diffusing through the precipitate film and the solution undergo a semi-infinite diffusion process (29) without migration effects (21, 22). Occurrence of metal ion concentration fluctuations in the film-solution interface will induce surface tension gradients capable of setting the film-acid solution system in motion. We shall make use of a linear stability analysis (23) to determine the hydrodynamic patterns formed in the region. As the basic state we shall consider that a constant flux of ions has been established in the quiescent fluid system. For the sake of simplicity we may assume that the precipitated layer (phase 1) is a Newtonian fluid of a viscosity higher than that of the semi-infinite solution (phase 2).

The full equations for the convective-diffusive process in the perturbed fluid system are given by the Navier-Stokes, the diffusion, and the continuity equations. To solve the above equations we adopt the usual procedure (18, 20, 23). As solutions to the equations we propose functions which have an exponential dependence with time ($\approx e^{\beta t}$) and a periodic transverse structure separable from the nonperiodic longitudinal one. In the determination of the stability of a hydrodynamic system it is convenient to search for the marginal states which separate the stable from the unstable regions (23). These states are characterized by the zeros of the real part of the growth constant β. We initially consider the problem for the real and the imaginary parts of β equal to zero.

Typically neutral stability curves obtained from the characteristic equations are shown in Fig. 2 (solid curves). These curves depend on the following parameters (18): the ratios μ_1/μ_2 and D_1/D_2 between the viscosities and diffusivities of fluids 1 and 2, the quasi-equilibrium distribution coefficient m between metal ion concentrations at the film-solution interface, and the product αd of the reciprocal of the perturbation length, α, and the film thickness d. The curves also depend on the dimensionless numbers: crispation group $N_{cr} = \mu_2 D_2/(\gamma_o d)$, surface viscosity group $N_{sv} = (\kappa + \epsilon)/(\mu_2 d)$, and Marangoni number $N_{Ma} = i\partial\gamma/\partial C\, d^2/(nFD_2^2\mu_2)$, where γ_o is the undisturbed value of the film-solution interfacial tension, κ and ϵ are the film-solution surface viscosities, i is the electrode current density, $\partial\gamma/\partial C$ is the derivative of the interfacial tension with respect to metal ion concentration in the solution side of the film-solution interface, n is the number of electrons involved in the electrochemical process, and F is the Faraday constant. The solid curves in Fig. 2 define two distinct regions of instabilities whether the Marangoni number N_{Ma} is positive ($\partial\gamma/\partial C > 0$) or negative ($\partial\gamma/\partial C < 0$). Each curve has two extrema; accordingly there are two critical N_{Ma} so that, for Marangoni numbers between them, all disturbances are

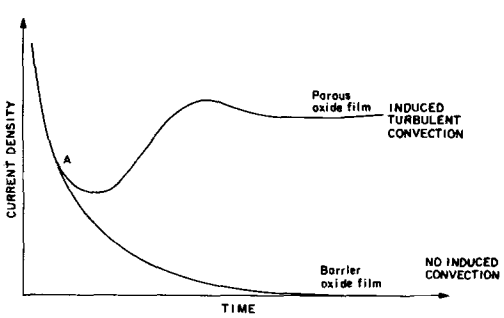

Fig. 1. Current density *vs.* time transient curves for the formation of barrier-type and porous-type anodic films on aluminum.

* Electrochemical Society Active Member.

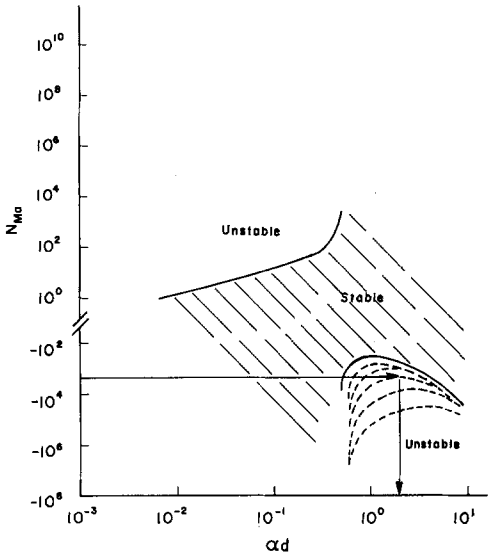

Fig. 2. Plot of the Marangoni number N_{Ma} (driving force/dissipative force) as a function of the product of the inverse of the perturbation length α, with the film thickness d. Solid lines are typically neutral stability curves that separate the stable from the unstable regions. Dashed lines represent the solutions of the characteristic equation for real positive values of the growth constant β. The arrows indicate schematically the procedure for obtaining the perturbation length of the fastest growing perturbation from a given Marangoni number.

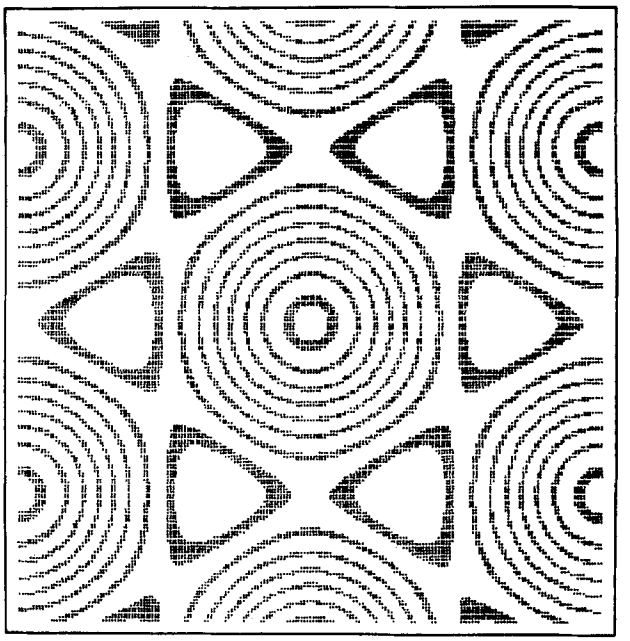

Fig. 3. Typical transverse cross section of the perturbated concentration profile for a hexagonal pattern.

damped. Another interesting feature of the neutral stability curves is that, for positive values of N_{Ma}, the system becomes unstable with respect to disturbances of great lengths ($\alpha d < 1$) and, for negative N_{Ma}, instability can set on for perturbations of small lengths ($\alpha d > 1$).

We have also solved the equation for real positive values of the growth constant β. From the solutions obtained we can predict the length of the dominant perturbation for a given set of physical parameters. Figure 2 schematically indicates the procedure for obtaining the length λ of the fastest growing perturbation for a given value of the Marangoni number [for definiteness, the perturbation length λ for a hexagonal cell pattern can be taken as the hexagon diagonal, so that $\lambda/d = 8\pi/(3\alpha d)$].

Starting from the solutions obtained for β real and positive, concentration, and velocity profiles can be calculated for a given set of parameters. The perturbation of concentration for a hexagonal pattern is shown in Fig. 3 and 4. Figure 3 shows the transverse cross section of the concentration perturbation formed at a distance $z = 0.9\ d$ from the electrode surface and Fig. 4 gives the longitudinal cross section of the perturbation. The transverse cross section of the fluid velocity inside the precipitated film is shown in Fig. 5.

Experimental

Apparatus and materials.—A diagram of the experimental apparatus used is shown in Fig. 6. Analytical grade reagents (Merck) were used without further purification. Aqueous H_2SO_4 solutions were prepared with twice-distilled water. The counterelectrode was a platinum 99.99% pure mesh with a submerged area at least 20 times greater than the area of the working electrode. Fresh electrodes and fresh solutions were used in every run. The anodization process was carried out in various concentrations of sulfuric acid solutions and in phosphoric, chromic, and oxalic acid solutions. The working electrodes were 99.9% aluminum wires with 2 mm diam (Varian) mounted in a PTFE support structure as shown in Fig. 6. The cylinder was placed a few tenths of a millimeter above the PTFE surface in order to prevent bubbles from covering the aluminum electrode. Experiments were also performed for aluminum samples covered by a silicone paste forming a pencil-like structure. The impurities detected by x-ray microprobe analysis were mainly silicon. The samples were mechanically polished with emery paper (grits 80, 140, 360, 500, and 1600) in order to remove mechanical inhomogeneities and then washed with chemical soap and water and rinsed with analytical grade methanol.

Before each experiment the samples were cleaned by: (*i*) optically polishing with diamond paste (Diamond Compound for Metallography—METADI), (*ii*) rinsing in distilled water, (*iii*) etching in NaOH (10 g/liter) for 30 min, (*iv*) rinsing in distilled water for 3 min, (*v*) immersion in HNO_3 (30%) for 15 s, (*vi*) rinsing in distilled water.

The dc voltage was generated by a Phillips Model PE 1512 stabilized power supply (35 V, 3.5 A). In order to keep the output voltage constant at the beginning of the anodization, electrolytic capacitors resulting in a total capacitance of 15,000 μF (connected by 150 kΩ resistors) were connected in parallel, as shown in Fig. 6. The current-time dependence is obtained by measuring the voltage across a 0.08 Ω resistance. The current *vs.* time signal is registered by a 7100 BM Hewlett-Packard strip recorder.

A few of the samples had their aluminum oxide layer removed by immersion in a solution of chromic acid (20 g/l) and 35 ml of phosphoric acid (85%/l) at 82°C for 5 min, for later observation by SEM.

A diagram of the experimental apparatus used for measuring the variation of the wettability states of aluminum electrodes were described previously (24, 25). The samples were electropolished with a low current density (~10 mA/cm^2) in a solution of methanol and perchloric acid (50:3). Tests were performed in sulfuric acid solutions, made up with twice-distilled water, at concentrations varying from 0.3 to 2.0*M*.

The topography and composition of the electrodes were examined by scanning electron microscopy (JEOL-TS-

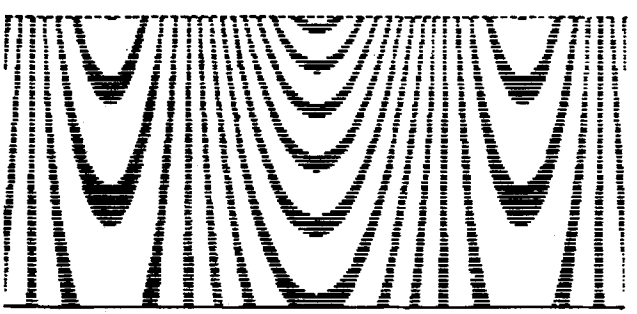

Fig. 4. Typical longitudinal cross section of the concentration profile.

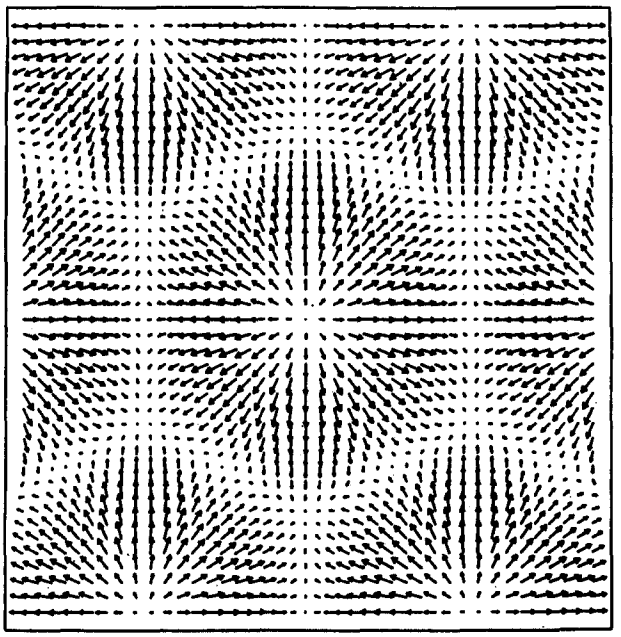

Fig. 5. Typical transverse cross section of the fluid velocity inside the formed film.

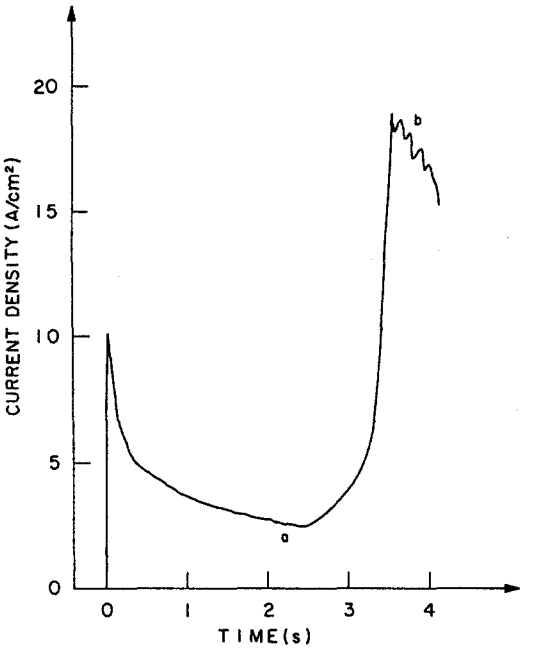

Fig. 7. Current density *vs.* time curve for a 22 V step application to aluminum in 20% H_2SO_4 solution.

300, 30 kV). The pictures were obtained by secondary electron imaging.

Results and Discussion

To obtain a sharp experimental pattern it is necessary to find the exact state at which pore initiation occurs and remove the sample from the solution at the first stages of the pore formation process. Figure 7 shows a current density *vs.* time curve observed experimentally for a constant voltage step. As the initial film precipitates, the current density decreases rapidly. At point a (Fig. 7) the current density reaches a minimum and, then, begins to increase. By SEM observation of the film morphology it could be established that a pattern could develop only for deposits removed from the electrolyte after the current has reached a minimum; pore initiation occurs then at some point close to a in Fig. 7. At the site of pore formation, a thinning of the barrier layer occurs, otherwise it would be difficult to account for the current density rise observed in our experiments. Sharper patterns are obtained for samples removed at some point close to point b.

Pattern formed on anodized aluminum.—Typical micrographs obtained for an aluminum electrode in contact with a 20% H_2SO_4 solution and anodized at 22 V are shown in Fig. 8a and b; no chemical etching procedure was applied to the electrode. The current density *vs.* time profile obtained for this sample is similar to the one shown in Fig. 7. The surface of an electrode submitted to a chemical etching procedure described in the Experimental section was also observed. The patterns were not formed in a regular arrangement like the ones shown in Fig. 8a and b.

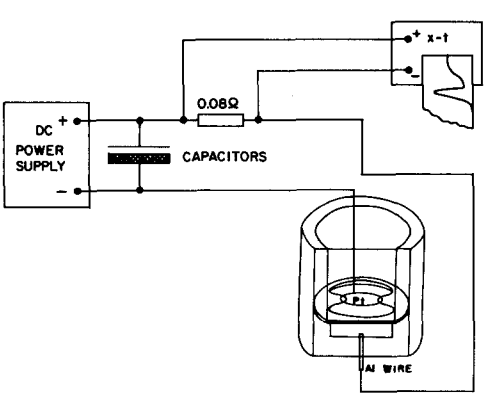

Fig. 6. Schematic diagram of the circuit and cell.

Figure 9a shows a cell pattern formed close to the edge of a cylindrically shaped electrode (Fig. 9b). Typical pattern dimensions are smaller for patterns closer to the electrode edge where the current density is higher. This indicates that the cell size is a decreasing function of the current density.

Patterns were obtained for various sulfuric acid concentrations and various current densities and the results are shown in Fig. 10 and 11. Figure 10 shows a plot of the average cell diameter measured by SEM, as a function of the acid solution concentration. Figure 11 shows a relation between the cell dimension and the electrode current density. A decrease in the cell dimension with increasing current density is obtained, as previously shown in Fig. 9.

The thickness of the initial precipitate layer can be estimated by considering Faraday's law for the aluminum dissolution process which occurs during the film formation stage. As discussed above, this stage lasts until the current attains its minimum value (point "a" in Fig. 7). In any estimate of this kind, two factors are of importance: (*i*) the current efficiency of the aluminum dissolution reaction at the anode and (*ii*) the composition and structure of the precipitate film. As regards (*i*), we estimate the current efficiency to be about 15% (1). Concerning (*ii*), we can assume that the film is formed by close-packed spherical particles immersed in an aqueous aluminum sulfate solution saturated in Al^{3+} (pH > 3), consequently the ratio between the total volume of the spheres and the volume of the surrounding solution is 68:32. For a formation process that lasts a few seconds only, the precipitating solid forming the particles is aluminum hydroxide which later is transformed into hydrous aluminum oxide. Due to lack of knowledge on the precise composition of the particles, we assume that they are composed of solid $Al(OH)_3$ with interspersed water molecules [typically 70 weight percent aluminum hydroxide (26)].

Allowing for all the inaccuracies on the knowledge of the above-mentioned factors, the thickness d of the layer laid down by the passage of a charge Q can be written as

$$d = \frac{f}{3F}\frac{Q}{Ac} \qquad [1]$$

where f is the current efficiency; F, as above, is the Faraday constant; A stands for the electrode area; and c is the total amount of Al^{3+} ions per unit film volume.

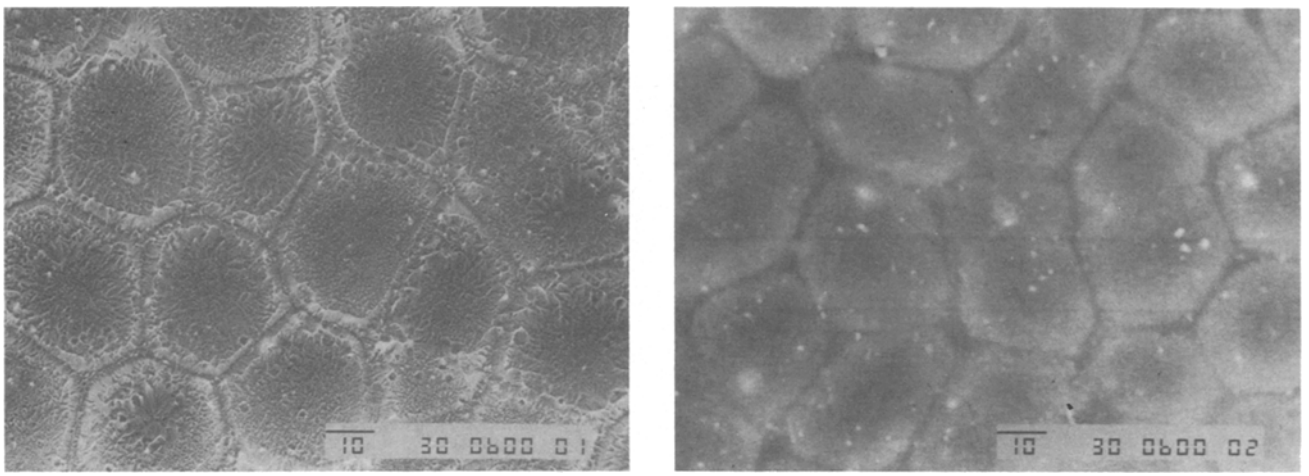

Fig. 8. Micrograph showing a patterned structure on an aluminum electrode in 20% H_2SO_4 anodized at 22 V: (a, left) secondary electron imaging and (b, right) backscattering electron imaging (BEI).

To estimate $\bar{c}$ with the help of the model proposed above we can consider the data found in the literature for the density [Ref. (27), p. B-68] and the solubility product of solid $Al(OH)_3$ (28).

Using our experimental data for Q/A obtained by integration of the current density *vs.* time curve up to point a and $\bar{c} \sim 10^{-2}$ mol/cm^3, we can get from Eq. [1] the film thickness. For example, a thickness $d \sim 23$ μm can be estimated from Eq. [1] for a film deposited on an aluminum sample anodized at 27 V in a 1*M* H_2SO_4 solution at 25°C ($Q/A \sim 47$ C/cm^2).

Electrode wettability measurements.—On aluminum electrodes there is always present an oxide coating even after prolonged evolution of hydrogen (25). Electrode wettability variations between this adjacent to the metal surface oxide coating (AMOC) and the coating formed at the anodic polarization were then measured. The experimental details can be found in Ref. (25).

The pull force measured for 0.3, 0.5, 1.0, 1.68, and 2.0*M* H_2SO_4 solutions is shown in Fig. 12 (25). The variation of the pull force with the electrode polarization shows a strong dependence on the acid concentration. We have also measured the pull force magnitude for pure aluminum electrodes in phosphoric, chromic, oxalic, and sulfuric acids. The synchronous component of the pull force (per unit length of the three-phase line) *vs.* time curves and the corresponding current-time curves for aluminum electrodes are shown in Fig. 13 for 15% sulfuric acid, 2% oxalic acid, 4% phosphoric acid, and 3% chromic acid. These results are used in Fig. 14 to show correlation for the various tested acids, between the ratio of the pull force variation to the anodizing current density and the product between the cell dimension (10) and the anodizing current density. Since the film thickness is essentially proportional to the reciprocal of the current density (21), we can easily see that the ratio of the pull force variation to the current density gives essentially the Marangoni number (driving force/dissipative force) while the product of the cell dimension and the current density at the anodizing potential represents the ratio of the cell dimension to the film thickness. Thus, Fig. 14 shows strong evidence of the relation between cause and effect in cell pattern formation, as predicted by our model (18).

Correlation between cell size and variation of interfacial tension.—As discussed above, the cell sizes found in the literature (12) and also observed in our experiments are correlated to (*i*) the amplitudes of the variation of the oxide-AMOC wettability in the aluminum anodization process and (*ii*) the anodizing current densities for the various acids investigated. These results suggest that cell formation on aluminum surfaces may be induced by wettability changes (for a given acid concentration and the current density at a given anodization potential). Accordingly, a correlation between the N_{Ma} obtained by using the experimentally determined pattern dimensions for various sulfuric acid concentrations and our model, and the N_{Ma} obtained from the pull force measurements can be established.

Determination of $\partial\gamma/\partial C$ from electrode wettability measurements.—The interfacial tensions γ_{sg} and γ_{lg} do not have a significant potential dependence (25), consequently the

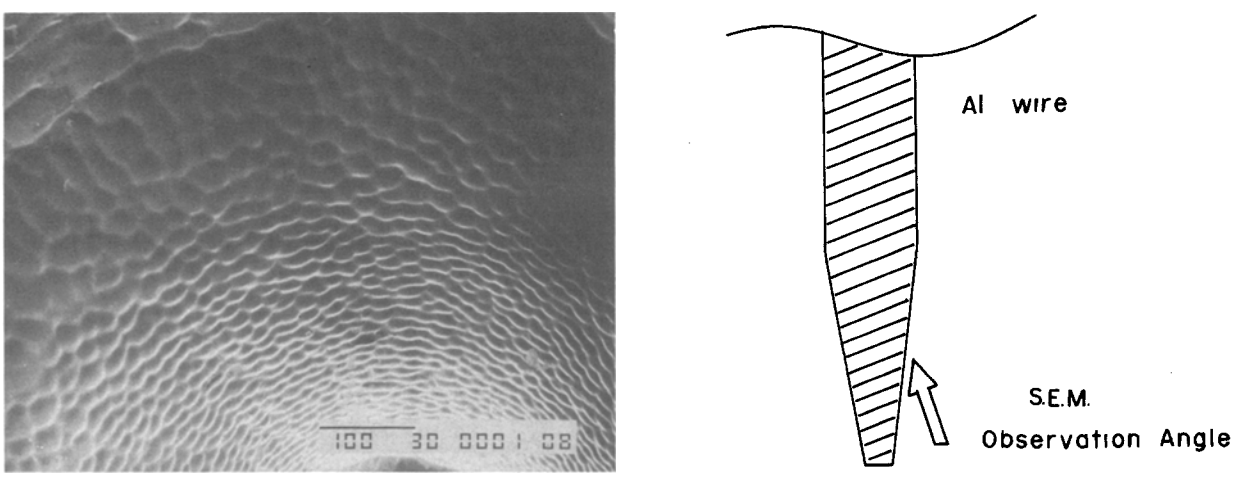

Fig. 9. (a, left) Cell pattern formed on a cylindrically shaped aluminum electrode close to its edge (sample anodized at 25 V in 1M H_2SO_4). (b, right) SEM observation angle.

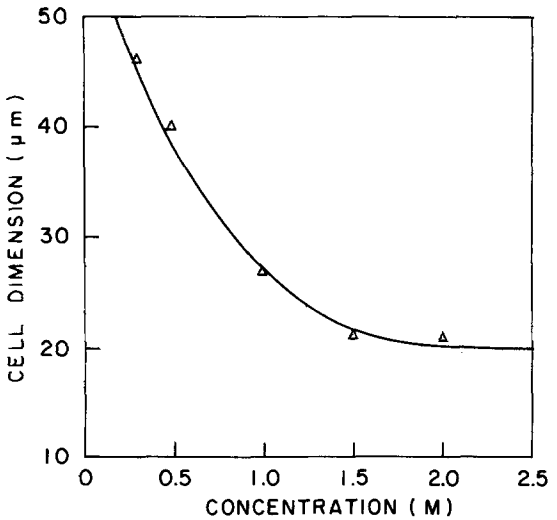

Fig. 10. Cell dimension *vs.* sulfuric acid concentration for aluminum anodized at 25 V in sulfuric acid concentrations at 25°C.

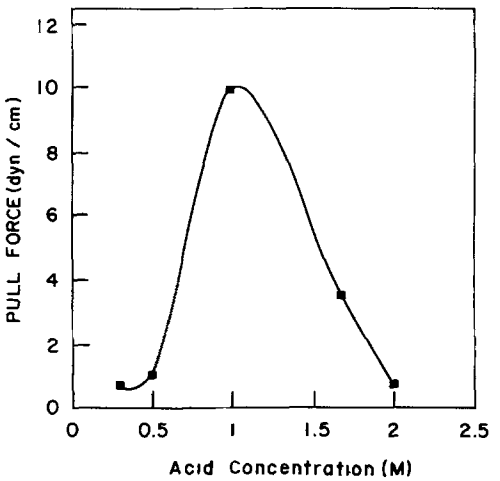

Fig. 12. Pull force as a function of sulfuric acid concentration for a 2.5 V *vs.* SCE anodic potential and a cathodic polarization resulting in a 200 μA cathodic current.

only interfacial tension altered in the transition AMOC (hydrogen evolution) to the anodization potential is γ_{sl}. The measured variation of the pull force ΔF is related to $\Delta\gamma_{sl}$ by $\Delta\gamma_{sl} = -\Delta F/2\pi r$ where r is the electrode radius.

For hydrogen evolution the electrode surface is not bare aluminum but is partially covered by an oxide film (AMOC); the concentration of Al^{3+} ions in the solution close to the electrode surface is practically zero after a time long enough for the ions formed in the previous anodization cycle to leave it by diffusion and convection. On the other hand, during anodization the electrode surface is covered by an increasing concentration of Al^{3+} ions which eventually precipitate into a layer. Consequently, the values obtained in our wettability measurements are proportional to the difference in the interfacial tension between the film-solution and AMOC-solution interface, *i.e.*

$$-\frac{\Delta F}{2\pi r} = \gamma_{\text{film-solution}} - \gamma_{\text{AMOC-solution}}$$

The experimental results (25) show that there is an increase in ΔF with time during the positive pulse duration and, consequently, a decrease of the interfacial tension with the increase of the aluminum oxide concentration formed by the anodizing current. According to our model (18), the driving force for the cell formation mechanism is the variation of the surface tension with the Al^{3+} concentration in the solution. Let us now estimate this variation. The electrode surface tension is a function of the solution concentration of the aluminum ion, C_{Al}, the sulfate ion concentration, which can be considered equal to the acid concentration, C_{ac}, in the bulk of the solution, and the applied electrode potential, V, *i.e.*, $\gamma_{sl} = \gamma_{sl}(C_{Al}, C_{ac}, V)$. The subscript sl will be dropped from now on since we will refer exclusively to γ_{sl}.

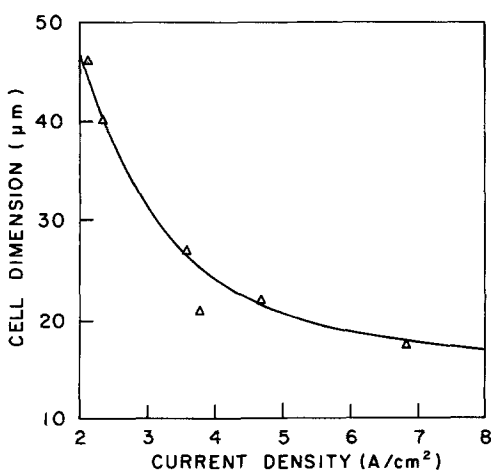

Fig. 11. Cell dimension *vs.* electrode current density for aluminum in various sulfuric acid concentrations at 25°C.

For the initial state at the hydrogen evolution potential we will use the subscript h and for the electrode state at the anodizing potential, the subscript a. The values of γ for these two states can be related by a Taylor expansion which, as a first-order approximation, reads

$$\gamma_h = \gamma_a + \left.\frac{\partial\gamma}{\partial C_{ac}}\right|_a \Delta C_{ac} + \left.\frac{\partial\gamma}{\partial C_{Al}}\right|_a \Delta C_{Al} + \left.\frac{\partial\gamma}{\partial V}\right|_a \Delta V \qquad [2]$$

where ΔC_{Al} is the difference in the aluminum ion concentration between the two electrode states, and ΔC_{ac} is approximately equal to zero. If we assume that, after 10 min of hydrogen evolution, the concentration of aluminum ions close to the electrode is negligible due to diffusion and convection and that the concentration at the electrode anodizing state is the saturation concentration, C_{sat}, we can write

$$\Delta C_{Al} = C_{Al}|_h - C_{Al}|_a = -C_{sat}$$

since both potential switching time and apparatus time response to pull force variations are around 1 s, pull force variation due to potential changes should be detected in a few seconds. However, what we observe is a rather gradual variation of the pull force up to ~10 min instead of an instantaneous contribution at each potential switching (from cathodic to anodic). Consequently the term $(\partial\gamma/\partial V)\Delta V$ can also be neglected in Eq. [2]. Then

$$\gamma_h \cong \gamma_a + \left.\frac{\partial\gamma}{\partial C_{Al}}\right|_a (-C_{sat})$$

Finally

$$\frac{\partial\gamma}{\partial C} \equiv \left.\frac{\partial\gamma}{\partial C_{Al}}\right|_a \simeq (\gamma_a - \gamma_h)/C_{sat} \qquad [3]$$

Determination of $\partial\gamma/\partial C$ using pattern dimensions for various solution concentrations.—The cells show predominantly a hexagonal pattern. The most probable hexagonal cell size given by the model is the one with the higher amplification factor γ. Accordingly, the product of the measured cell dimension with the layer width determines the N_{Ma} value in the N_{Ma} *vs.* αd curve, as shown in Fig. 2.

The experimentally determined values of αd are greater than 3.0, consequently the values of $\partial\gamma/\partial C$ obtained from the model have a negative sign, in agreement with the sign

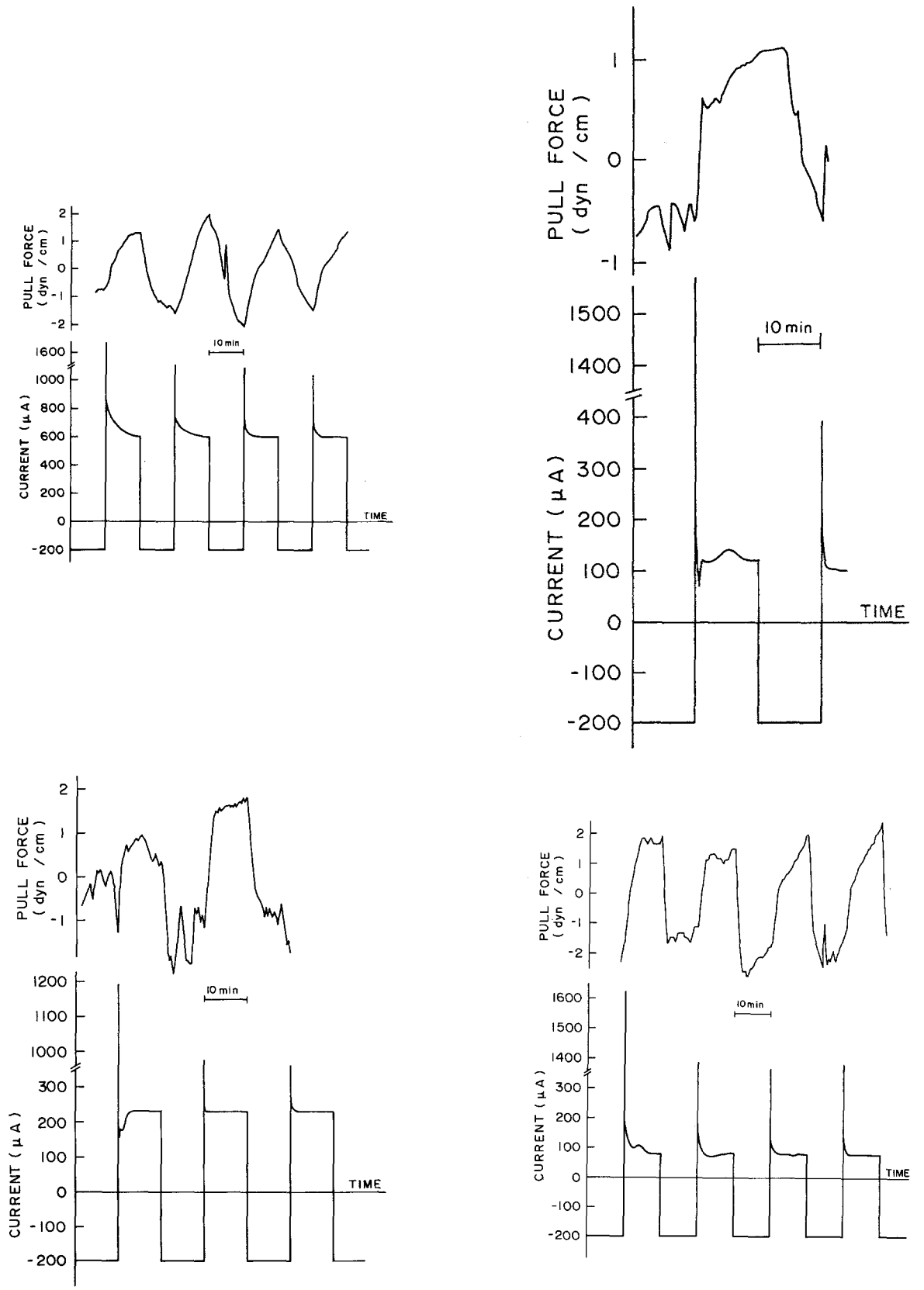

Fig. 13. Synchronous component of the pull force per unit length of the three-phase line *vs.* time and the corresponding current-time curves for aluminum electrodes in (a, top left) 15% sulfuric acid, (b, top right) 2% oxalic acid, (c, bottom left) 3% chromic acid, and (d, bottom right) 4% phosphoric acid.

measured experimentally. The value of $\partial\gamma/\partial C$ is determined by the expression

$$\frac{\partial\gamma}{\partial C} = \frac{N_{Ma}\mu_2 nFD_2^2}{id^2}$$

obtained from (18).

The following numerical values were taken in the calculations: density ρ_2 and viscosity μ_2 of sulfuric acid solutions at various concentrations from Ref. (27), p. D-263; aluminum ion diffusion coefficient in solution: $D_2 \sim 4.5 \times 10^{-6}$ cm^2/s [in analogy to Fe^{3+} data from Ref. (29)]. Colloidal layer density is $\rho_1 \sim 1.5$ g/cm^3; film-solution viscosity ratio $\mu_1/\mu_2 = 10$, and diffusion coefficients ratio $D_1/D_2 = 0.1$. The

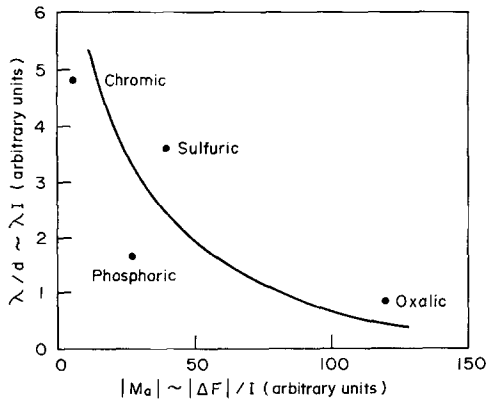

Fig. 14. Correlation between the Marangoni number (pull force variation/anodic current density) and the ratio of the cell size to film thickness (cell size times anodic current density) for aluminum electrodes in 4% phosphoric, 3% chromic, 2% oxalic, and 15% sulfuric acid for periodically switched potentials (anodic +2.5 V *vs.* SCE cathodic and 200 μA current).

Al^{3+} concentration ratio m in the film and the electrolyte was taken to be equal to 1 and the colloidal-solution interfacial tension 1000 dyn/cm.

The surface viscosities were adjusted such as to obtain a coincidence better than 98% between the measured $\partial\gamma/\partial C$ values and the calculated values using the experimental cells dimensions. The values for $(\kappa + \epsilon)$ obtained for different solutions concentrations are, respectively, 2.5×10^{-2}, 1.7×10^{-2}, 2.5×10^{-2}, and 8.2×10^{-4} sP, for concentration values of 0.3, 0.5, 1.0 and 2.0*M* H_2SO_4 solutions, respectively. The surface viscosity values obtained were between 10^{-4} and 10^{-2} sP, in agreement with Ref. (30). This strongly indicates that the mechanism of cell formation is related to solute concentration inhomogeneities at the film-solution interface through local variations in the film-solution interfacial tension. Consequently weak capillary forces induce electrolyte convection in the vicinity of the electrode surface and determines the patterns which emerge when a more viscous layer is formed over the electrode surface.

The question of why do porous films initiate faster in sulfuric acid than in phosphoric acid (2) can thus be answered: our experimental results show that $\partial\gamma/\partial C$ is larger for sulfuric than for phosphoric acid, consequently, according to our model, the cell growth coefficient is larger for sulfuric acid than for phosphoric acid.

Now referring to the reason why low coating ratios are experimentally observed (2), it would be difficult to distinguish between aluminum going directly into solution without recourse to oxide, and aluminum in solution resulting from oxide surface dissolution. Our hydrodynamic model shows that larger fluid circulation velocities imply small cell dimensions and that the oxide deposition at preferential sites is simultaneous with the formation of pores. Thus the circulation of the electrolyte is the main factor on the deposit structure.

Another point worth mentioning is the difficulty of conceiving why the ratio of aluminum going directly into solution to the aluminum going toward oxide formation should be such a strong function of temperature. Surface tension is known to be strongly temperature dependent (31). Our model shows that the driving force for the cell formation are surface tension inhomogeneities; thus cell dimensions can also present a strong temperature dependence.

Finally, our model also explains why very thin oxide layers are free of pores. Deposits formed at a high current density result in thin films (<0.1 μm thick) and it is energetically unfavorable to set the fluids into motion to form cells in such thin layers.

Conclusion

In this work a correlation was found between the size of cells formed during aluminum anodization and the measured variation of surface tension between the hydrogen evolution reaction potential region and the anodizing potential region. The model proposed in our previous paper (18) establishes a relation between $\partial\gamma/\partial C$ and the cell size for iron electrodes in H_2SO_4 solutions. A relation was found experimentally for aluminum electrodes in sulfuric, oxalic, phosphoric, and chromic acids thus suggesting that the driving force for the cell formation mechanism is a combination of the electrode current density and $\partial\gamma/\partial C$, as expressed by the Marangoni number. A correlation was also established for various sulfuric acid concentrations.

In conclusion, our results indicate that weak capillary forces act as singular perturbations which induce electrolyte convection in the vicinity of the electrode surface and determine the patterns which emerge when a more viscous layer is formed over the electrode surface. The formation of a barrier-type oxide layer corresponds to a range of values of the Marangoni number for which perturbed hydrodynamic and diffusion equations have no solutions, in other words, convection is ineffective.

Acknowledgments

This work was supported by grants from Fundação de Amparo a Pesquisa do Estado de São Paulo (FAPESP) and CNPq. M.U.K. is grateful to FAPESP for financial support.

Manuscript submitted Nov. 19, 1990; revised manuscript received April 24, 1991.

Instituto de Fisica-UNICAMP assisted in meeting the publication costs of this article.

REFERENCES

1. J. W. Diggle, T. C. Downie, and C. M. Goulding, *Chem. Rev.*, **69**, 365 (1969).
2. G. E. Thompson and G. C. Wood, in "Treatise on Material Science and Technology," Vol. 3, J. C. Scully, Editor, Academic Press, London (1983).
3. T. P. Hoar and J. Yahalom, *This Journal*, **110**, 614 (1963).
4. R. W. Franklim, Paper presented at "Conference on Anodizing Aluminum," Nottingham, 1961, Aluminum Development Association (1961).
5. D. T. Arrowsmith, E. A. Cupan, and P. J. Smith, in "Proceedings of the International Symposium on Anodizing Aluminum," Birmingham (1967).
6. J. P. O'Sullivan and G. C. Wood, *Proc. R. Soc. London. Ser. A*, **317**, 511 (1970).
7. J. S. Leach and P. Neufeld, *Corros. Sci.*, **9**, 413 (1969).
8. P. Neufeld and H. O. Ali, *Trans. Inst. Metal Finish*, **48**, 175 (1970).
9. H. Ginsberg and K. Wefers, *Metall.*, **16**, 1973 (1962); **17**, 202 (1963).
10. F. Keller, M. S. Hunter, and D. L. Robinson, *This Journal*, **100**, 411 (1953).
11. C. E. Michelson, *ibid.*, **115**, 213 (1968).
12. G. C. Wood, in "Oxides and Oxide Films," J. C. Diggle, Editor, Marcel Dekker, Inc., New York (1973).
13. S. Wernick, *J. Electrodep. Tech. Soc.*, **9**, 153 (1934).
14. W. Baumann, *Z. Phys.*, **102**, 59 (1936); **111**, 707 (1939).
15. J. F. Murphy and C. E. Michelson, in "Proceedings of the Conference on Anodizing Aluminum," Nottingham, 1961, Aluminum Development Association (1961).
16. K. V. Heber, *Electrochim. Acta.*, **23**, 127, 135 (1978).
17. O. Teschke, D. M. Soares, and M. U. Kleinke, *Langmuir*, **5**, 1162 (1989).
18. M. A. Tenan, O. Teschke, M. U. Kleinke, and F. Galembeck, *ibid.*, **6**, 1640 (1990).
19. The mechanism would be similar to that considered for the iron electrode; see T. R. Beck, *This Journal*, **129**, 2412 (1982); J. H. Bartlett and L. Stephenson, *ibid.*, **99**, 504 (1952); A. Pigeaud and H. B. Kirpatrick, *Corrosion*, **25**, 209 (1969).
20. C. V. Sterling and L. E. Scriven, *AIChE J.*, **5**, 514 (1959).
21. R. Alkire, D. Ernsberger, and T. R. Beck, *This Journal*, **125**, 1382 (1978).
22. R. Alkire and A. Cangellari, *ibid.*, **130**, 1252 (1983).
23. S. Chandrasekhar, "Hydrodynamic and Hydromagnetic Stability," Chap. 2, Oxford University Press, London (1961).
24. O. Teschke, M. U. Kleinke, and F. Galembeck, *Langmuir*, **5**, 844 (1989).
25. O. Teschke, M. U. Kleinke, and M. A. Tenan, *This Journal*, **137**, 781 (1990).

26. F. Galembeck, Private communication.
27. "CRC Handbook of Chemistry and Physics," 66th ed., R. C. Weast, Editor, CRC Press, Boca Raton, FL (1985).
28. J. Bjerrum, G. Schwarzenbach, and L. G. Sillén, "Stability Constants, Part II: Inorganic Ligands," pp. 20, 21, The Chemical Society, London (1958).
29. A.-M. Baticle, F. Perdu, and P. Vennereau, *C. R. Acad. Sci., Paris*, **264**, 12 (1967).
30. A. W. Adamson, "Physical Chemistry Surfaces," 4th ed., p. 118, Wiley, New York (1982).
31. A. W. Adamson, "Physical Chemistry Surfaces," 4th ed., p. 51, Wiley, New York (1982) and "CRC Handbook of Chemistry and Physics," 66th ed., R. C. Weast, Editor, p. F-32, CRC Press, Boca Raton, FL (1985).

Thermodynamic Study of Proton Insertion into Thin Films of Amorphous WO_3

M. Rezrazi, B. Vuillemin, and O. Bohnke*

Laboratoire d'Electrochimie des Solides (U.A. 0436 CNRS), Universite de Franche-Comté, 25030 Besancon, France

ABSTRACT

The formation of hydrogen tungsten bronzes, H_xWO_3, prepared electrochemically from thin films of amorphous WO_3, has been thermodynamically studied. The variation of the chemical potential of the inserted species in these thin films of oxide at ambient temperature has been measured using an electrochemical method. The reduction of the amorphous oxide, corresponding to the reaction

$$a\text{-}WO_3 + {}_xH^+ + xe^- \rightarrow H_xWO_3$$

proceeds in a homogeneous phase, as shown by the shape of the E *vs.* x curve. We shall point out in this paper that it is necessary to consider insertion of proton-electron pairs into the oxide instead of considering the formation of a mixed oxide. A theoretical treatement of the E *vs.* x curve allows us to determine the repulsive interaction between the inserted species as insertion occurs and the influence of the electronic term on the potential.

The formation of hydrogen tungsten bronze phases H_xWO_3 by chemical reduction of either polycrystalline samples of WO_3 (1) or hexagonal WO_3 (2, 3) has been widely studied. Much less work has been done on electrochemically formed hydrogen tungsten bronzes. Hitchman (4) has studied the equilibrium potentials of samples of crystalline WO_3 films. He has shown that the oxidation of bronzes by oxygen is thermodynamically strongly favored and that the bronzes are in a fully ionized state, *i.e.*, the hydrogen bronze can be regarded as being in a dissociated state $[H_xWO_3 \rightarrow xH^+ + xWO_3^- + (1-x)WO_3]$. Jarman *et al.* (5) have studied polycrystalline WO_3. They have shown that tetragonal phases are formed during electrochemical reduction of this material as obtained during chemical reduction. Finally, Crandall *et al.* (6) have studied the insertion of protons into amorphous WO_3 thin films and determined a theoretical expression of the chemical potential of hydrogen from the free energy of formation of one mole of H_xWO_3. It is necessary to notice that the electrochemical reduction of amorphous thin films of WO_3 compared to crystalline material is of a great importance because of the total reversibility of the insertion reaction and consequently because of its potential use for electrochromic passive information displays (7, 8) glare-free rearview mirrors for automotive (9), solar control windows (10-12), and thermal sensors (13). In the remainder of the paper we will refer to amorphous thin films of WO_3 as a-WO_3.

In a crystalline oxide, single-phase regions and two-phase regions may be observed on the E *vs.* x curve corresponding to a change in the crystalline structure of the oxide during cathodic insertion. On the other hand, we can observe that the reduction of the amorphous oxide proceeds in a homogeneous phase. The reaction may be expressed as

$$a\text{-}WO_3 + xH^+ + xe^- \rightarrow a\text{-}H_xWO_3 \qquad [1]$$

In the present work, the variation of the chemical potential of the inserted species in amorphous tungsten trioxide thin films has been measured using an electrochemical method. A theoretical treatment of the E *vs.* x curve allows us to determine the repulsive interaction between the inserted species as insertion occurs and the influence of the electronic term on the potential. Moreover, we shall point out that it is necessary to consider insertion of proton-electron pairs into the oxide instead of considering the formation of a mixed oxide.

Experimental Procedure

The experimental technique used in this work to obtain hydrogen tungsten bronzes of varying hydrogen concentration is an electrochemical technique which has been described first by Thompson (14). The experiment is performed in the following ways. The electrochemical cell, initially in equilibrium, is connected to a constant potential power supply (potentiostat) set at $E = Eequ.$; the power supply is then stepped to a more cathodic potential, a current crosses the cell as insertion proceeds; when the current reaches a value equal to $Io/100$ (with Io = initial current), the power supply is then stepped again. The values of E (potential) and Q (injected charge) at the stepping point are measured with the automated equipment. The advantage of using this technique compared to the galvanostatic method is that much less time is required and the possible degradation of the tungsten oxide electrode by the acid medium is avoided. Computer-controlled equipment for data acquisition is used. The experimental setup is shown in Fig. 1. The potentiostat (Schlumberger 1186) is

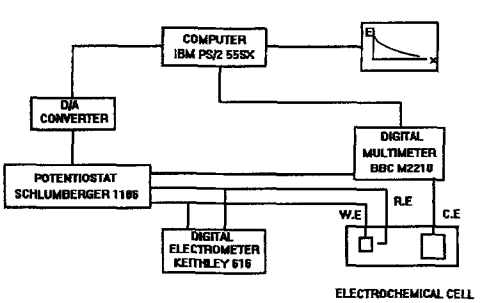

Fig. 1. Schematic diagram of the experimental setup.

* Electrochemical Society Active Member.